Remote Sounding of High Clouds. III: Monte Carlo Calculations of Multiple-Scattered Lidar Returns

C. M. R. PLATT

CSIRO Division of Atmospheric Physics, Aspendale, Victoria, Australia 3195

(Manuscript received 4 April 1980, in final form 2 September 1980)

ABSTRACT

Monte Carlo calculations of multiple-scattered contributions to the total energy received in a lidar beam have been made for a representative cirrus ice-cloud scattering phase function. The phase function is varied arbitrarily near the back direction to give three different scattering patterns. The Monte Carlo method of Plass and Kattawar (1971) has been modified and extended to give a greatly increased efficiency for a small decrease in accuracy. This modification has reduced the computation time by ~80%, allowing routine calculations to be made on many different cloud models. When applied to two water cloud models the method gives results which agree well with those obtained by previous workers. The purpose of the calculations is to investigate the apparent reduction in the cloud optical depth due to multiple scattering when measured by a lidar. This reduction is described here by a multiple scattering factor η. It is found that for cirrus clouds the factor η varies considerably with the depth of cloud penetration, with the cloud optical depth and with the cloud extinction coefficient.

The calculations show for the first time the pattern of contribution from each order of scattering separately. It is shown that for cloud optical depths ≥ 0.1 a model which considers double scattering only is inadequate.

1. Introduction

The effectiveness of lidar sounding of high cirrus clouds, particularly when combined with passive infrared (IR) measurements, has now been well established (Davis, 1971; Platt, 1973, 1979; Platt and Dilley, 1979).

It became apparent soon after the first measurements on clouds were made that the multiple-scattered component in the lidar return was appreciable and that it complicated the interpretation of the lidar backscatter amplitudes. Platt (1973) demonstrated that a backscatter to extinction ratio $k/2\eta$ could be extracted from a plot of the integrated attenuated lidar backscatter against IR emissivity, where k is the true backscatter to extinction ratio and η is a multiple scattering factor. Combination of the lidar and infrared data enabled Platt (1973) to extract a value of η of 0.41 ± 0.15, thus making it possible to obtain a value of k. A problem with obtaining such a value of η from experiment is that it gives no information on the possible *variations* of η with the geometrical, or optical, depth of the cloud or with the cloud particle type. At present the measured cloud backscatter coefficient is corrected for pulse attenuation by using a single experimental value of $k/2\eta$ to obtain the cloud visible extinction coefficient at the lidar wavelength (Davis, 1971; Platt, 1979). Any variation of the value of η with cloud depth will obviously cause errors in the calculated extinction coefficient.

The multiple-scattered component in the lidar beam has been computed previously by the Monte Carlo technique [e.g., Plass and Kattawar, 1971 (PK); Kunkel and Weinman, 1976 (KW)]. The Monte Carlo technique enables the full calculation of the multiple-scattered returns, including all significant orders of scattering. PK and KW investigated the multiple scattering from vertically homogeneous water clouds and found a variation of η with cloud penetration.

The problem with the Monte Carlo method as used by the above authors is that it is very costly in computer time, as well as being subject to considerable noise in the results. The reason lies in the lidar geometry and the difference in the directional anisotropy between the forward and backscatter properties of the cloud particles. Photons are scattered into the back hemisphere fairly isotropically. However, the very few photons which *are* scattered close to the back (180°) direction can subsequently undergo a near-forward scatter with a probability of reaching the lidar receiver which is much higher than average. Unless very many photons are investigated, the total energy returned to the laser receiver will both be underestimated and subject to large fluctuations.

This article describes a method of conditioning the

0022-4928/81/010156-12$07.00

Monte Carlo method specifically for the lidar problem by weighting the backscatter in such a manner that a large number of high-probability photons are allowed to contribute. This artifice reduces considerably the computation time needed to attain a satisfactory signal-to-noise ratio in the result. The method is used to calculate the effect that multiple scattering has on the lidar measurement of high-cloud optical depth (Platt, 1979). The altitudes, thicknesses and optical depths of typical ice clouds are simulated in the model. A representative ice-cloud phase function is chosen from an investigation of the theoretical and experimental work which has been done so far.

2. Ice-cloud scattering phase functions

Our knowledge of the characteristics of ice-cloud phase functions is at present rather sketchy and derived wholly from a few laboratory measurements together with some theoretical calculations.

Dugin *et al.* (1971) measured variations in scattering function which they attributed to differing crystal structures. They observed platelets, prisms and stars but could not relate the scattering functions uniquely to crystal type. Huffman (1970) made observations from 10° to 150° scattering angle on plates, irregular crystals and columns. Liou *et al.* (1976) and Sassen and Liou (1979) measured the phase function for ice needles, columns and plates. Liou (1972) computed the phase function for infinitely long, randomly-oriented cylindrical ice needles. Jacobowitz (1971) computed the scattering from hexagonal crystals, which were assumed to be randomly oriented in one plane, by ray-tracing methods.

The curves of these authors, for unpolarized radiation, are summarized in Fig. 1; they are normalized at 90° scatter angle. The curves are broadly consistent in the 5 to 90° region but differ in the 0 to 5° region, where diffraction effects make the results sensitive to crystal size, and in the 90 to 180° region, where the results become sensitive to crystal type and orientation.

The strong influence of crystal size, shape and orientation on the shape of the phase function is likely to cause significant differences in the multiple scattering characteristics of various ice clouds. The work contained in the present series of articles is concerned with high cirrus ice clouds which occur at temperatures mainly below −25°C (e.g., Platt and Dilley, 1979). Crystals sampled in these clouds have been found to be mainly hexagonal in form. The 22° halo, often seen in the solar scattering pattern of cirrus clouds, is also indicative of hexagonal crystals. There is evidence too, that these ice crystals fall with their long axes horizontal.

In order to obtain some preliminary results on the multiple scattering characteristics of cirrus clouds, it was thus decided to use Jacobowitz's published phase function, as this was the only study on hexagonal crystals available at the time that the present work was commenced. Jacobowitz's phase function is for hexagonal crystals with their long axes randomly oriented in the horizontal plane and with vertical illumination.

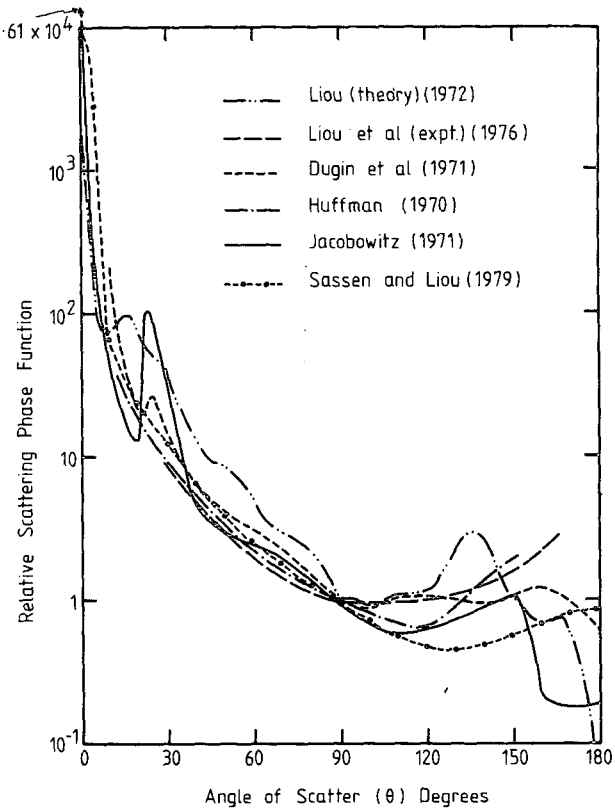

FIG. 1. Measured and calculated relative scattering phase functions for ice crystals.

Wendling *et al.* (1979) have recently found from a study similar to that of Jacobowitz that the phase function increases markedly in amplitude near the back direction. However, this will depend in practice on whether the crystals fall with one of their six plane faces in the horizontal and also whether the crystals fall exactly horizontally (e.g., Platt *et al.*, 1978). Because of possible variations in backscatter, variations which are also evident in the curves of Fig. 1, it was decided to arbitrarily modify the Jacobowitz phase function in the 150 to 180° region in three different ways, thus forming in effect three different phase functions. A preliminary study had previously shown that such a variation had a marked effect on the multiple scattering contributions. The three variations are shown in Fig. 2.

The amplitude of the forward diffraction peak will also affect the multiple scattering contributions. The

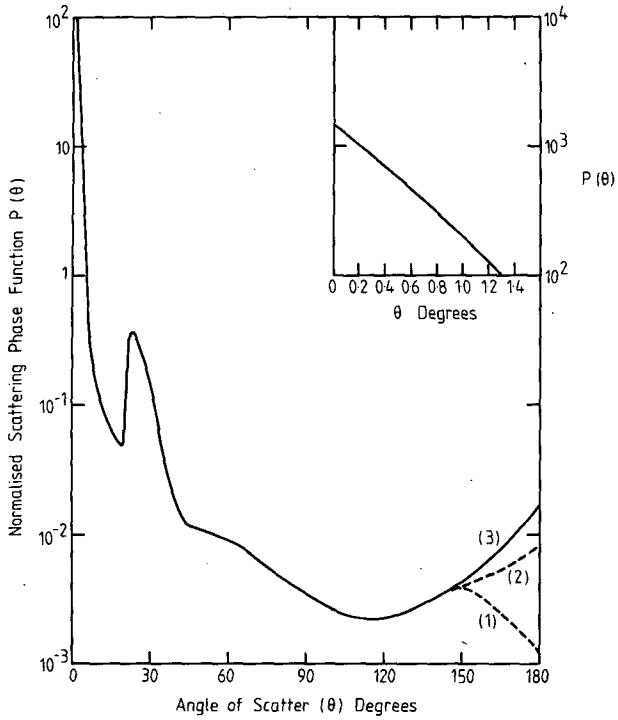

FIG. 2. Scattering phase function for cirrus adopted for the present work. The curves near the back direction for series 1, 2 and 3 are marked accordingly.

present Jacobowitz phase function has a value of $P(0)$ which represents ice crystals having dimensions of ~50 μm on the long axis. The value of $P(0)$ is actually an order of magnitude greater than that reported by Sassen and Liou (1979) but an order of magnitude less than those reported by Wendling *et al.* (1979) for 240 μm long columns. The influence of these considerable variations in the diffraction peak on the multiple scattering factor will be pursued in a future article.

3. Monte Carlo simulation

a. The calculation

The Monte Carlo calculation follows that of PK and KW in some respects but with several innovations which increase the efficiency of computation dramatically with only a minor reduction in accuracy.

The scattering geometry is illustrated in Fig. 3. Single photons are projected upwards into the cloud from a transmitter within a cone of half-angle θ_m. It is assumed that the lidar is vertical. The intensity distribution of photons within the cone is made uniform, the angle of transmission of each photon being thus chosen as $\theta = \theta_m(\mathrm{RF})^{1/2}$ where RF is a random number between 0 and 1. Effects of Rayleigh and aerosol scattering are neglected so that the intensity distribution in the receiver beam at the surface is unchanged from that at cloud base. Efficiency of computation is achieved, as in PK, by forcing each photon to scatter before reaching the limits of a specified volume defined by the cloud base and cloud top and a vertical conical section, symmetrical about the transmitter cone, and corresponding to a selected receiver angle. In order to compensate for this artificial behavior, the probability of the photon which is directly scattered onto the receiver detector following each scatter is suitably reduced. Photons are scattered repeatedly within the receiver cone until their probability of reaching the receiver detector at each scattering is reduced below a value of 10^{-6}.

Once inside the cloud, the depth at which the first scattering event occurs, L_1 (=PQ), is given by

$$L_1 = (1/\sigma)\log_e\{1/[1 - \mathrm{RF}(1 - \tau_1)]\}. \quad (1)$$

where σ is the cloud particle extinction coefficient and τ_1 the transmittance from cloud base to cloud top along PM.

The distance to subsequent scattering events is similarly given by

$$L_i = (1/\sigma)\log_e\{1/[1 - \mathrm{RF}(1 - \tau_i)]\}, \quad (2)$$

where τ_i is the transmittance from the previous scattering event to the scattering limits. Each time that a first scattering event occurs the probability p_1 of a photon reaching the detector D directly is estimated as

$$p_1 = [P(\psi_1)A/z_1^2]\exp[-\sigma(z_1 - z_0)](1 - \tau_1), \quad (3)$$

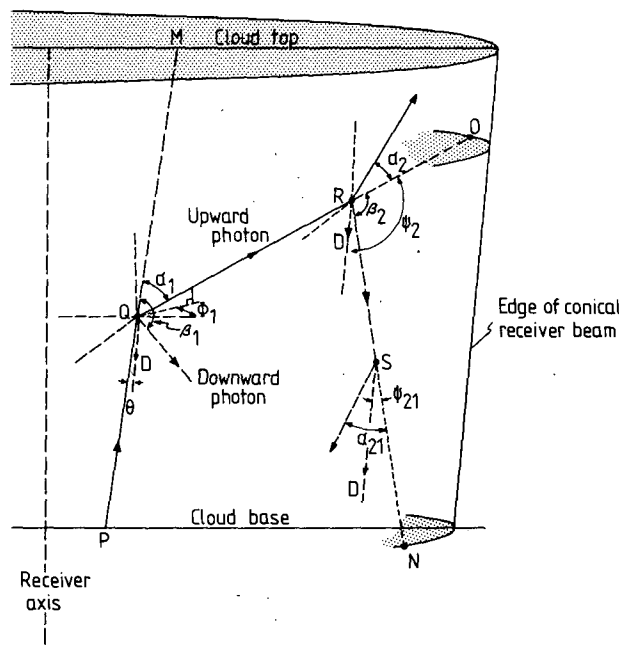

FIG. 3. Schematic of photon scattering from cloud particles within the lidar receiver beam.

TABLE 1. Lidar parameters used in the water cloud comparisons.

Comparison	σ (m^{-1})	z_0 (m)	Receiver aperture half-angle ϵ (rad)	Transmitter half-angle θ_m (rad)	Cloud
Eloranta[1]	0.0168	1000	0.005	0.005	C1
Kunkel and Weinman (1976)	0.010	1000	0.005	0.0001	C1
Kunkel and Weinman (1976)	0.010	1000	0.005	0.0001	Nimbostratus

[1] Eloranta, E. W., 1972: Calculation of doubly scattered lidar returns. Ph.D. thesis, University of Wisconsin, 115 pp.

where A is the receiver area, z_1 the altitude (range) of the scatter point and z_0 the range at cloud base altitude. $P(\psi_1)$ is the normalized scattering phase function at an angle of scattering ψ_1 $(=180 - \theta_1)$.

b. First modification

So far the method has followed the Monte Carlo codes of PK and KW. The first modification consists of treating upward and downward scattered photons separately. Each time that a scattering event occurs, both cases are considered, with suitably reduced probabilities. For the downward scattered photon, only scattering in the forward hemisphere is pursued. This procedure introduces only small errors because the overall probability of a photon being scattered into the back hemisphere is small (~4%) so that a downward travelling photon that is subsequently scattered upwards has very little chance of reaching the detector. First order estimates of these errors were always less than 1% of the total probability. An upward travelling photon which suffers two large-angle scatters and thereby reverses direction is treated as a normal downward travelling photon.

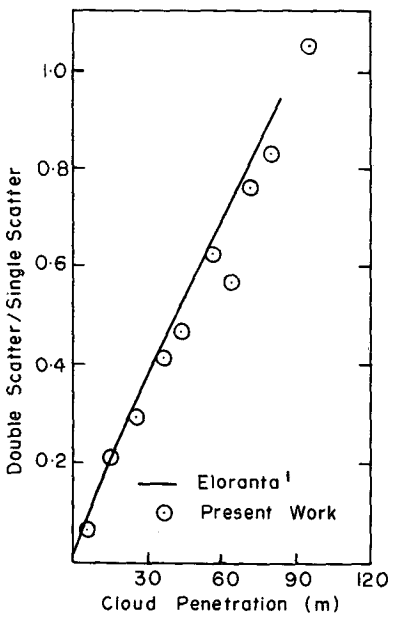

FIG. 4. Ratio of double to single scatter obtained in the present study for Deirmendjian model cloud C1 compared to the analytical result of Eloranta.

At each scatter, the upward travelling photon is scattered into the forward hemisphere at an angle α from the incident photon direction, decided randomly by an angular probability distribution function derived from the scattering phase function (McKee and Cox, 1974, Kunkel and Weinman, 1976), and at an azimuth angle ϕ $[=2\pi(\mathrm{RF})]$ from the plane of incidence. This photon has a reduced probability given by $(1 - w')$, where w' is the fraction of photons scattered into the back hemisphere, as calculated from the relevant phase function. The probability p_2 of the upward photon reaching the receiver after a second scatter at R is

$$p_2 = [P(\psi_2)A/z_2^2] \exp[-\sigma(z_2 - z_0)] \times (1 - \tau_1)(1 - \tau_2)(1 - w'). \quad (4)$$

where τ_2 is the transmittance along the photon path from Q to O (Fig. 3), the edge of the receiver beam.

Similarly, at each scatter the downward travelling photon assumes a direction β to the incident direction which is decided by a (normalized) backscatter probability distribution. This procedure itself is inefficient and a "conditioning" of the normalized backscatter angular distribution function is described below.

c. Second modification

The second modification, and in fact the major innovation introduced here involves the appropriate conditioning of the photon path in the back hemisphere. Scatter in the back hemisphere from ice crystals is much more nearly isotropic than forward scattering (Fig. 2). If the unmodified probability distribution for backscatter is used, photons will tend to be scattered rather equally at all angles in the back hemisphere, and only a very few photons will follow close to the back direction. However, it is just these photons scattered near 180° and subsequently rescattered during their downward travel, which give a very high probability at the detector, compared to photons scattered at larger angles from the 180° direction. The final result is that the total

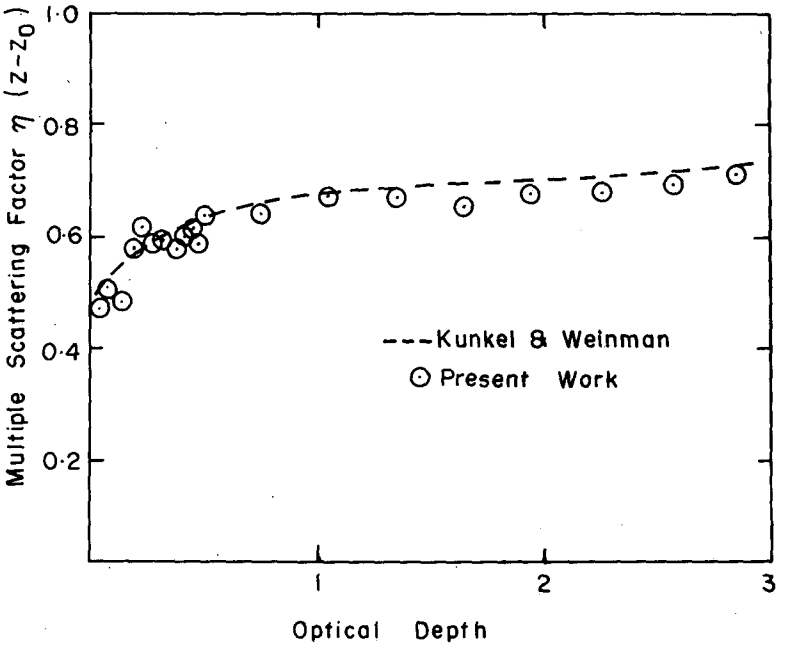

FIG. 5. Multiple scattering factor $\eta(z - z_0)$ obtained for cloud C1 in the present study compared with the result of Kunkel and Weinman. The broken line represents a line drawn by hand through their points of $\bar{F}(z_0')$ $(=1 - \eta)$.

computed probabilities contain "spikes" of very high values from certain random levels in the cloud. If more photons are used in the computation then the probability at the detector from each level builds up, as eventually the proper number of high values are received from each level. In the first runs, it was found that after using 2000 photons, the "spikes" were very evident and over 10 000 photons were needed before the probability built up to a reasonably smooth function with altitude. These "spikes" have also been noted by Golubitskiy and Tantashev (1973) for similar calculations.

The above procedure is obviously a very inefficient way to compute probabilities for the lidar geometry and it can lead to an underestimation of multiple scattered returns if sufficient photons are not used. It was thus decided to condition the backscatter in such a way that many photons would proceed near the back 180° direction but with an appropriately reduced probability. In fact, photons were scattered in the back direction using the *forward* probability function, where the angle of scatter $\beta = (180 - \gamma)$, γ being the selected forward angle. The photon probability was then weighted by a function $F(\beta)$ which was the ratio of the rate of change of the normalized backscatter probability distribution at the angle β to the rate of change of the normalized forward scatter probability at the angle γ.

Thus for a photon scattered downwards at S (Fig. 3), the probability p_{21} at the detector is

$$p_{21} = (P(\psi_{21})A/z_{21}^2) \exp[-\sigma(z_{21} - z_0)] \times (1 - \tau_1)(1 - \tau_2)(1 - \tau_{21})F(\beta_2)(1 - w')w', \quad (5)$$

where z_{21} is the distance of S to the receiver detector D and τ_{21} is the transmittance from R to the edge of the receiver beam at N (or alternatively, to the cloud base).

The above procedure, using 2000 photons, was found to give similar results as a computation with the original unmodified backscatter, which used 10 000 photons, and no "build-up" of probability could be detected as the number of photons was further increased. The computation time was thus reduced by a factor of 5.

d. Probabilities of photon scattering

For practical calculations the cloud is divided vertically into ten equally-spaced layers and it is assumed that photons scattered from any level within each layer come from the center level of the layer. It can be shown that this linear averaging within each layer is a valid procedure. The total probabilities for each order of scattering and for each cloud layer are recorded during a computation.

Allowance also has to be made for photons which are scattered out of the receiver cone and subsequently scattered back into the cone (KW). The probability at the detector from such photons was estimated by making a second run, with a cone five times larger than the original receiver cone. The

probability of photons scattered out and then returning in to the receiver cone could then be estimated by computing the probability from such photons using an "inner" receiver cone. The probability for such photons was then added to the probability of multiple scattering made in the previous run, making allowance for the different probabilities for *total* multiple scattering for the two cone sizes.

For reasons that will be explained in Section 4 only the relative probabilities at various levels are required, so that the energy received at the detector from any cloud level, as a fraction of the transmitted energy, need not be calculated.

4. Lidar equation and multiple scatter

The general methods and theory for deriving the cloud backscatter coefficients and for calibration of a lidar are given in Part I of this series (Platt, 1979). For a calibrated lidar system, the measured attenuated isotropic cloud backscatter coefficient $B_c'(\pi,z)$ at an altitude z is related to the unattenuated value by the expression

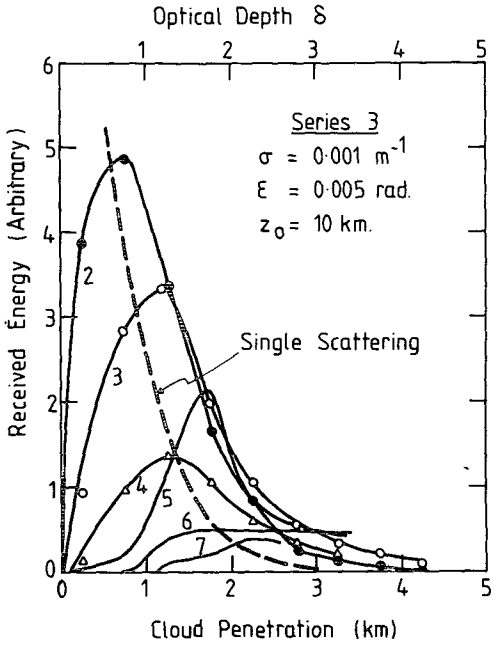

FIG. 7. The relative received energies in different orders of scattering for the cirrus cloud model.

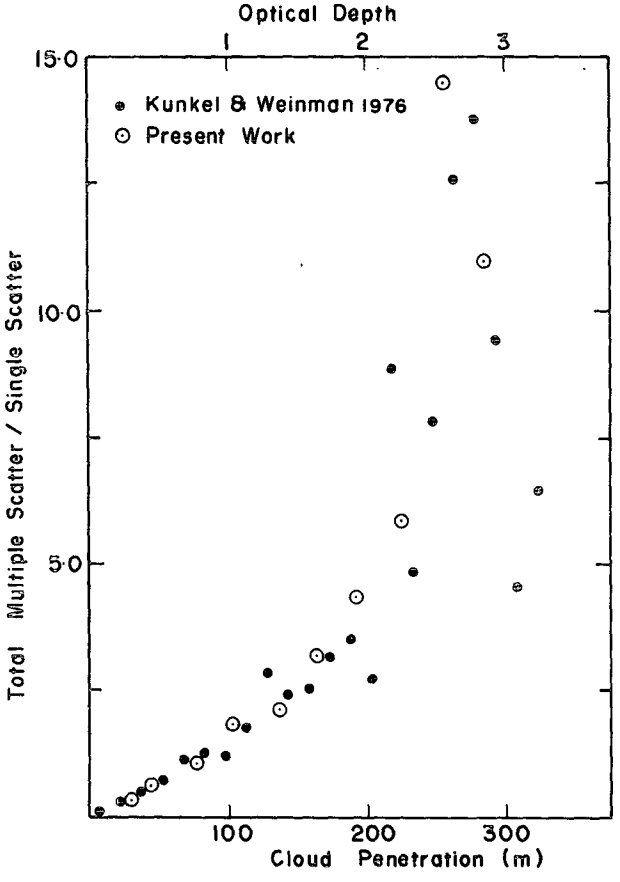

FIG. 6. The ratio of total multiple scatter to single scatter obtained for the nimbostratus Deirmendjian cloud model, compared to the points obtained by Kunkel and Weinmann.

$$B_c'(\pi,z) = B_c(\pi,z)\exp\left[-2\eta(z-z_0)\int_{z_0}^{z}\sigma(z'')dz''\right], \quad (6)$$

where z_0 is the cloud-base altitude and $\eta(z-z_0)$ is a multiple scattering factor which describes the reduction in optical depth between z_0 and z due to multiple scattering, as defined in Platt (1979). It is assumed that the lidar is sounding vertically.

The quantity $\eta(z-z_0)$ can be calculated from the relative multiple scattering probabilities as follows. Let the backscatter coefficient in Eq. (6) be termed $B_c'(\pi,z)(TS)$, the TS indicating total scattering. Consider the case when only single scattering (SS) occurs. Then

$$B_c'(\pi,z)(\mathrm{SS}) = B_c(\pi,z)\exp\left[-2\int_{z_0}^{z}\sigma(z'')dz''\right], \quad (7)$$

and therefore,

$$\frac{B_c'(\pi,z)(\mathrm{TS})}{B_c'(\pi,z)(\mathrm{SS})} = \frac{\exp\left[-2\eta(z-z_0)\int_{z_0}^{z}\sigma(z'')dz''\right]}{\exp\left[-2\int_{z_0}^{z}\sigma(z'')dz''\right]}, \quad (8)$$

from which

$$\eta(z-z_0) = 1 - \log_e[(B_c'(\pi,z)(\mathrm{TS})/B_c'(\pi,z)(\mathrm{SS})]\left[2\int_{z_0}^{z}\sigma(z'')dz''\right]^{-1}. \quad (9)$$

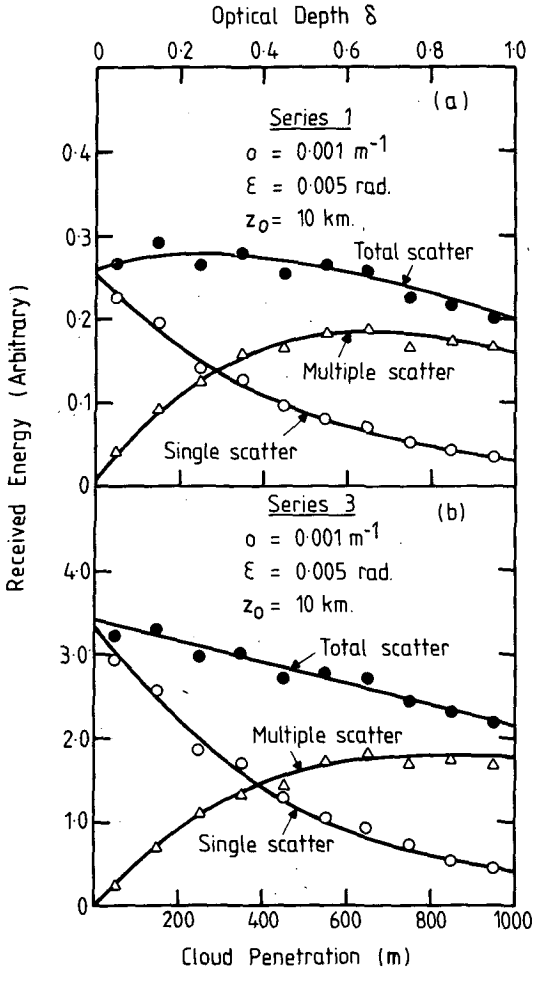

FIG. 8. Comparison of the contributions of single-scattered and multiple-scattered energy to the total scattering for two cases of the cirrus cloud model.

The quantities $B_c'(\pi,z)$(SS) and $B_c'(\pi,z)$(TS) are proportional to the computed probabilities (at altitude z) for single scattering and total scattering respectively so that they can be obtained directly, for any cloud layer, from the Monte Carlo results.

Consider now the total integrated backscatter $[\gamma'(\pi)]$ through the cloud:

$$\gamma'(\pi) = \int_{z_0}^{z_T} B_c'(\pi,z)dz, \qquad (10)$$

where z_T is the cloud top altitude.

If η is not a function of z then, using Eq. (6), the integral of Eq. (10) has a simple solution of the form (Platt, 1973)

$$\gamma'(\pi) = k/2\eta\left\{1 - \exp\left[-2\eta\int_{z_0}^{z_T}\sigma(z'')dz''\right]\right\}, \qquad (11)$$

where k is the isotropic backscatter to extinction ratio (see next section). As the integral (or optical depth) in Eq. (11) becomes large, then $\gamma'(\pi)$ tends to $k/2\eta$.

If η is a function of z then the solution of Eq. (11) becomes complex and its behavior will be discussed in a future article. However, we can still consider the case where the optical depth tends to infinity. The integral $\gamma'(\pi)$ will now tend to a value $k/2\bar{\eta}(h)$, where $\bar{\eta}(h)$ depends on the form of $\eta(z - z_0)$, and h is the cloud depth. Since the quantity $k/2\bar{\eta}(h)$ can be measured from experiment (Platt, 1979) it is a useful quantity to be able to predict.

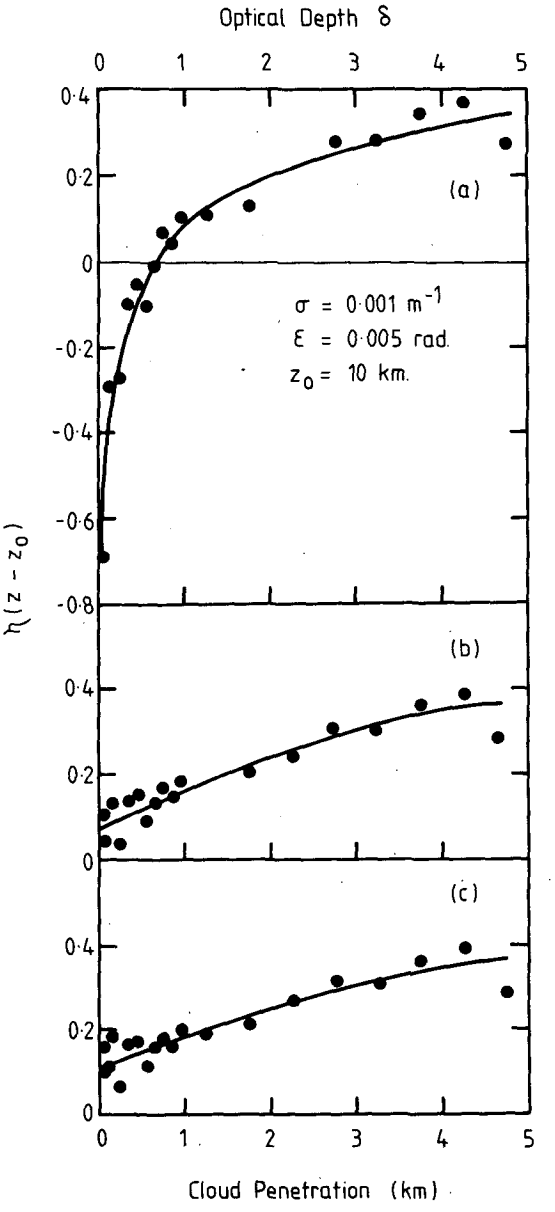

FIG. 9. Variation of the multiple scattering factor $\eta(z - z_0)$ with cloud penetration $(z - z_0)$ for the three series of the cirrus cloud model and for the geometries shown, ϵ is the receiver half-angle: (a), (b), (c) refer to series 1, 2 and 3, respectively.

We now let

$$\left.\begin{aligned}\gamma'(\pi)_\infty(\mathrm{SS}) &= k/2 \quad [\eta = 1 \text{ for single scattering}]\\ \gamma'(\pi)_\infty(\mathrm{TS}) &= k/2\bar{\eta}(h),\end{aligned}\right\},$$

where $\gamma'(\pi)_\infty$ refers to the case where the optical depth is large. Then,

$$\bar{\eta}(h) = \gamma'(\pi)_\infty(\mathrm{SS})/\gamma'(\pi)_\infty(\mathrm{TS}) \qquad (12)$$

$\gamma'_\infty(\pi)(\mathrm{SS})$ and $\gamma'_\infty(\pi)(\mathrm{TS})$ are here proportional to the single scattering and total scattering probabilities when summed through an optically thick cloud. It is thus possible to also obtain values of $\bar{\eta}(h)$ directly from the Monte Carlo results.

5. Backscatter to extinction ratio

The isotropic backscatter to extinction ratio k for a non-absorbing particle is defined by

$$k = \int_0^{4\pi} P(\pi)d\Omega \Big/ \int_0^{4\pi} P(\theta)d\Omega, \qquad (13)$$

where $P(\theta)$ is the normalized scattering phase function at angle θ. The denominator is the integrated normalized scattering intensity through a complete sphere and is therefore equal to unity. Thus

$$k = 4\pi P(\pi). \qquad (14)$$

We define here a second parameter E which we term the backscatter effectiveness

$$E = \int_0^{2\pi} P(\pi)d\Omega \Big/ \int_0^{2\pi} P(\theta)d\Omega$$

$$= 2\pi P(\pi) \Big/ \int_{\pi/2}^{\pi} P(\theta)\sin\theta d\theta. \qquad (15)$$

TABLE 2. Calculated values of $\bar{\eta}(h)$, k, $k/2\bar{\eta}(h)$ and E. z_0 = 10 km.

	Series number		
	(1)	(2)	(3)
k	0.016	0.108	0.205
E	0.45	2.83	5.05
(1) h = 5 km, σ = 1 km^{-1}			
(a) ϵ = 0.001 rad			
$\bar{\eta}(h)$	0.412	0.438	0.442
$k/2\bar{\eta}(h)$	0.019	0.123	0.232
(b) ϵ = 0.005 rad			
$\bar{\eta}(h)$	0.209	0.267	0.277
$k/2\bar{\eta}(h)$	0.038	0.202	0.370
(2) h = 1 km, σ = 5 km^{-1}			
(a) ϵ = 0.001 rad			
$\bar{\eta}(h)$	0.273	0.316	0.324
$k/2\bar{\eta}(h)$	0.029	0.171	0.316
(b) ϵ = 0.005 rad			
$\bar{\eta}(h)$	0.175	0.239	0.251
$k/2\bar{\eta}(h)$	0.045	0.225	0.408

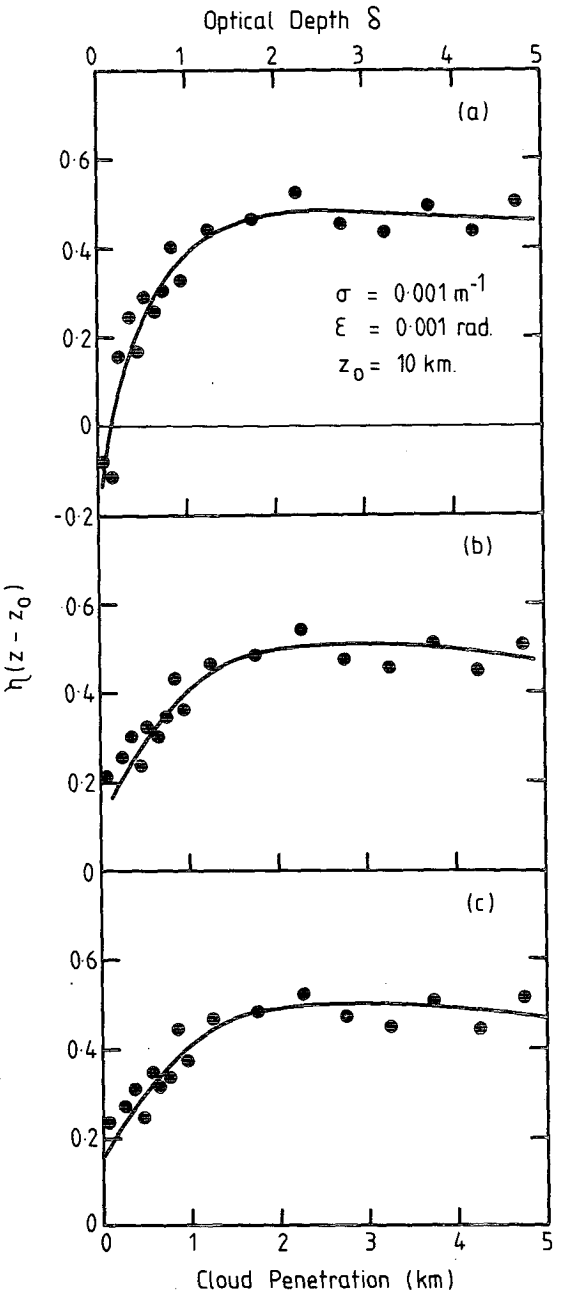

FIG. 10. As in Fig. 9, but for different geometries.

E is thus the ratio of the isotropic backscatter at 180° to the total scatter in the back hemisphere.

6. Comparison of the present Monte Carlo code with previous studies

In order to check the methods used here, a comparison was made with the results of two other authors. KW used Monte Carlo techniques to investigate multiple scattering in a lidar beam using the

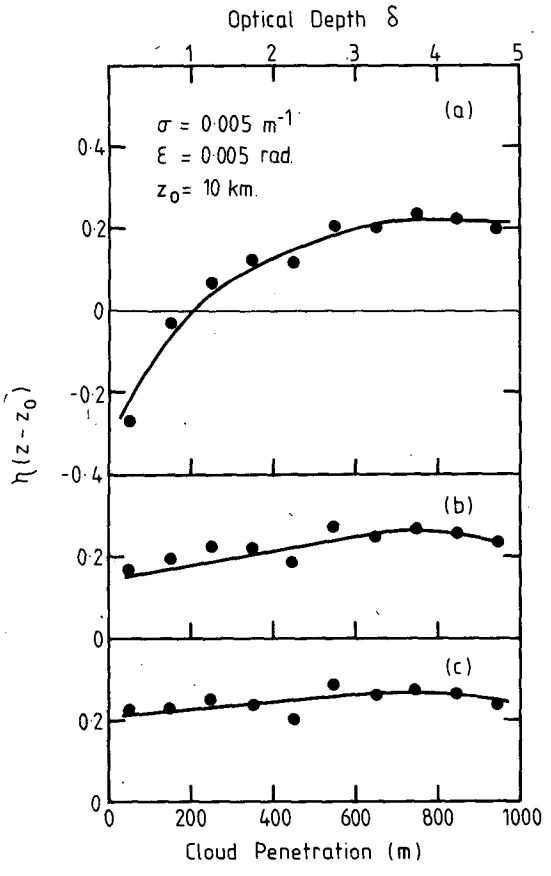

FIG. 11. As in Fig. 9, but for different geometries.

single scattering phase functions for both the Deirmendjian C1 and the nimbostratus water cloud models (Deirmendjian, 1964). Eloranta[1] worked out analytic relationships between lidar geometry and double scattering for the Deimendjian cloud C1 model. In order to test the present Monte Carlo model against the results of the above authors, calculations were done with both the Deirmendjian C1 and nimbostratus single scattering phase functions. The characteristics of these phase functions have been given by KW. The lidar and cloud parameters used in the comparisons are shown in Table 1. They were made to coincide with the parameters used by the above two authors.

The results of the comparison, using 2000 photons for each run, are shown in Figs. 4 to 6. The calculated ratios of double to single scattered returns are compared with the analytical expression of Eloranta in Figure 4. The agreement between the two methods is quite good. The second comparison is shown in Fig. 5 where values of $\eta(z - z_0)$ for the C1 cloud are compared with the values of $1 - \bar{F}(x_0')$ obtained by KW, where $\bar{F}(x_0') = 1 - \eta(z - z_0)$. The dashed line is the result of drawing a line of best fit through KW's experimental values. Again, the agreement is quite good, although the values of η at the higher optical depths are slightly lower than those obtained by KW. These authors did not use the backscatter conditioning used in the present study and their results may have been affected by the 'spike' phenomenon which, as well as giving them a fairly noisy result, would also give a value for η which was rather greater than the correct value.

The final comparison shown in Fig. 6 is the ratio of total multiple scattering to single scattering for the nimbostratus cloud. The agreement here is very good. Once again, the lower noise in the present model is evident.

The overall agreement in the above comparisons lends confidence to the following results on high ice clouds.

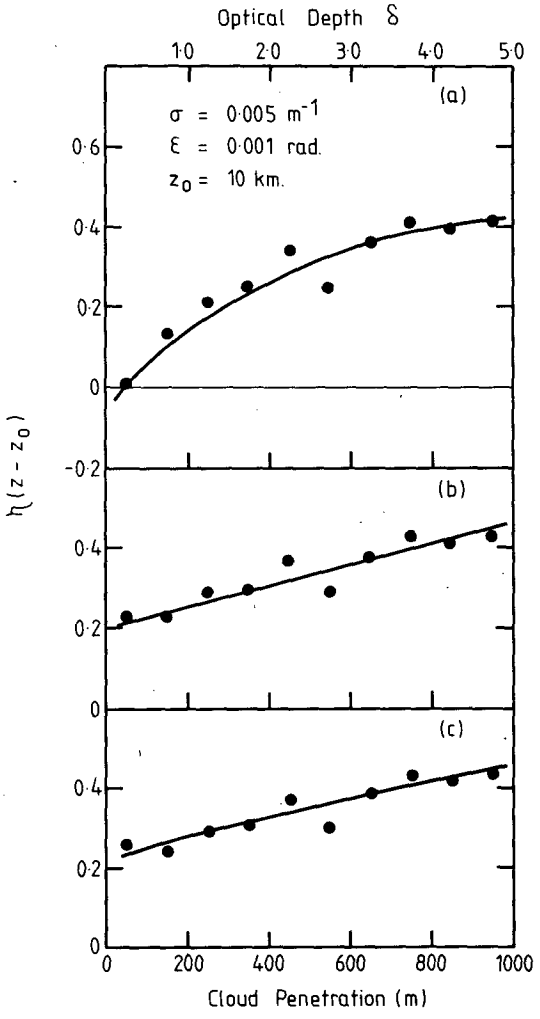

FIG. 12. As in Fig. 9, but for different geometries.

[1] Eloranta, E. W., 1972: Calculation of doubly scattered lidar returns. Ph.D. thesis, University of Wisconsin, 115 pp.

7. Results

The three phase functions of Fig. 2 were used for all calculations. They were divided into 1° intervals, except between 0 and 1° scattering angle when 0.1° intervals were used and between 1 and 2.5° where 0.5° intervals were used. The cloud was divided into 10 equal height intervals in the vertical. 2000 photons were used for each run. The clouds were assumed to be homogeneous with specified values of σ which were considered to be characteristic of cirrus clouds (Platt, 1973, Platt and Dilley, 1979). The transmitter aperture θ_m was set at 0.001 radians for all runs.

Results were calculated for each version of the phase function in Fig. 2. They are termed "series 1, 2 and 3", respectively. In practice, the different values near the back direction changed the values of $P(\theta)$ over the rest of the angular range slightly,

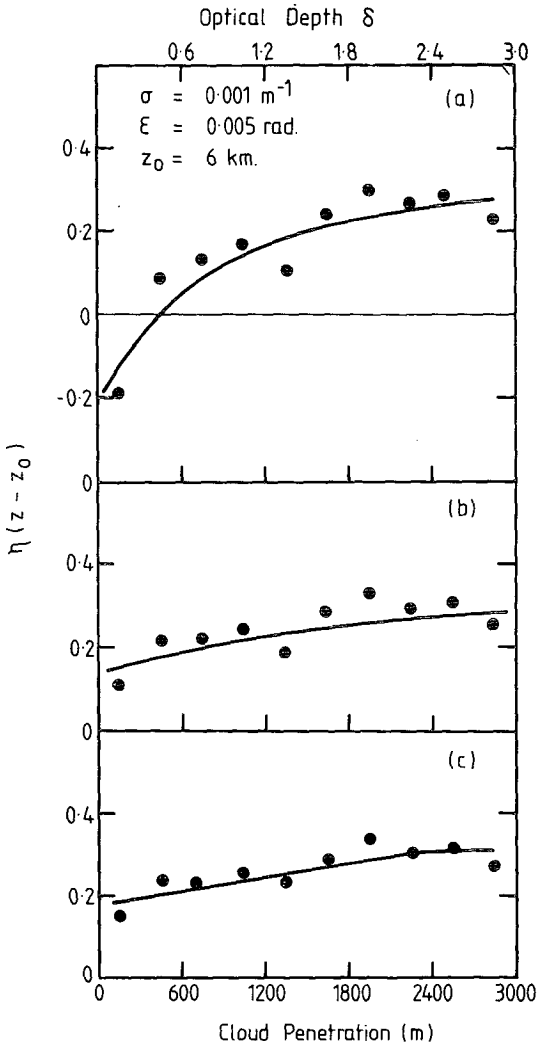

FIG. 13. As in Fig. 9, but for 6 km altitude cloud base.

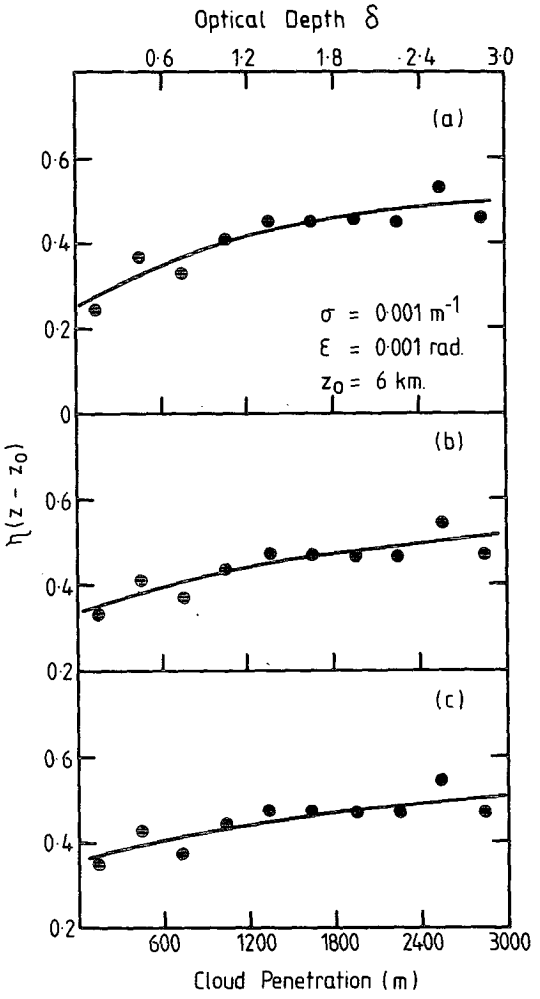

FIG. 14. As in Fig. 9, but for 6 km altitude cloud base.

and it was necessary to renormalize the value of $P(\theta)$ for each series. Fig. 2 shows the correct values for series 3.

The program format allowed the calculation of the probability of received energy for each order of scattering separately. Fig. 7 shows the contributions from each order for one particular case. It is evident that the contributions from scattering orders greater than 2 become rapidly very significant, even at optical depths below unity. This indicates, as substantiated by KW's results, that a double-scattering approximation is valid for only a very limited range of optical depths. It is interesting that the contributions from each order become approximately equal to those of every other order as the cloud optical depth is increased.

Fig. 8 shows the contributions of multiple and single scatter to the total scatter for series 1 and 3 and for the same lidar parameters as Fig. 7. Fig. 8a shows an interesting effect in that for penetration depths less than ~600 m, the total received energy

is *greater* than what would be expected from single scatter if there were *no* attenuation. This enhancement leads to *negative* values of $\eta(z - z_0)$, as shown in Fig. 9a, where the lidar parameters are the same as in Fig. 8, but where the total penetration depth is much greater. The negative effect occurs only for the series 1 phase function. This represents a case where the backscatter value $P(\pi)$ is less than the average in the back direction [i.e., the value of E is less than unity (Table 2)]. It is not difficult to see that in this situation, the total multiple scatter can become greater than the unattenuated single scatter, particularly near the cloud base. Figs. 9b and 9c show that the negative effect has disappeared for series 2 and 3 although $\eta(z - z_0)$ still increases almost monotonically with cloud depth. The random scatter of points about the full lines (i.e., "the noise") is a characteristic of the Monte Carlo method. Fig. 10 shows equivalent values of $\eta(z - z_0)$ when the lidar receiver aperture ϵ has been reduced from 0.005 radians to 0.001 radians. The aperture is then equal to the transmitter beamwidth. It is evident that even with this narrow aperture, there is still considerable multiple scattering and for series 1 there is still a residual enhancement effect near the cloud base. At an optical depth of about 2, the value of $\eta(z - z_0)$ levels off at a value of ~0.5 and then gradually declines.

Figs. 11 and 12 show the equivalent curves for an extinction coefficient σ of 0.005 m^{-1}. This value is large and the cloud will become rather opaque to the laser pulse at a penetration depth of 1 km, despite the effects of multiple scattering. The enhancement effect is still evident near the cloud base for series 1, but to a smaller penetration depth than for the less attenuating cloud. In series 2 and 3, Fig. 11 shows that $\eta(z - z_0)$ is fairly constant, but with a low value of ~0.2. When the aperture is narrowed, Fig. 12 shows that for series 2 and 3 there is still rather a monotonic increase in the value of $\eta(z - z_0)$.

Figs. 13 and 14 show equivalent curves for a cloud with its base at 6 km. Comparing Figs. 10 and 14, the most striking difference is that the sharp fall-off in $\eta(z - z_0)$ towards the cloud base is no longer apparent, although the value of $\eta(z - z_0)$ still approaches ~0.5.

Values of isotropic backscatter to extinction ratio k and effectiveness E, multiple scattering factor $\bar{\eta}(h)$ and the effective backscatter to extinction ratio $k/2\bar{\eta}(h)$ are shown in Table 2 for the three series. $\bar{\eta}(h)$ has been calculated from Eq. (12) using the ratios of $\gamma'(\pi)$(SS) to $\gamma'(\pi)$(TS) deduced from the Monte Carlo calculations when the total cloud optical depth was 10.

It is apparent that for a given cloud thickness $\bar{\eta}(h)$ is quite sensitive to the receiver aperture. Similarly, for a given aperture, $\bar{\eta}(h)$ is sensitive to the cloud depth. The value of k is directly proportional to the values of $P(\pi)$ ($\theta = 180°$) in Fig. 2. Similarly, the value of k varies directly with the value of E, as expected.

Finally, it should be noted that Allen and Platt (1977) measured an angular distribution of intensity in the transmitter beam which was closer to Gaussian, rather than a uniform distribution. A run was thus done with this type of photon distribution and for one set of conditions. This was found to cause negligible changes in the values of the multiple scattering factor η.

8. Discussion

Although it is clear from Fig. 1 that there is yet no definitive scattering phase function for high ice clouds, and no indication of how this function will change with particle size and type, the Jacobowitz profile of Fig. 2 should reproduce the general features of the multiple scattering factor for cirrus clouds.

First, the multiple scatter is seen to be very sensitive to the form of the phase function near the back direction; this is particularly true of the variation in $\eta(z - z_0)$ through the cloud. Whether a negative $\eta(z - z_0)$ can ever be observed in practice will depend on whether such low back-scatter phase functions occur. The experimental curve of Dugin *et al.* (1971) given in Fig. 1 indicates that these might be possible. Of course, it also will depend on the shape and magnitude of the forward diffraction peak, i.e., the particle size. This aspect is under investigation at present.

Apart from the observations of the scattering phase functions shown in Fig. 1, the only measured values of backscatter known to the author are those of Platt (1973), Sassen (1978) and Sassen and Liou (1979). The lidar measurements of Platt gave a value of 0.26 ± .06 for k and 0.41 ± 0.15 for $\bar{\eta}(h)$. The receiver aperture was 0.005 radians. The mean cloud thickness was 1.2 km. A glance at Table 2 indicates that for series 3, $\bar{\eta}(h)$ is predicted to be ~0.25 for these conditions. However, the value of 0.205 for k is still less than the measured value of 0.26, indicating that the backscatter may be even more peaked than shown by series 3.

Sassen (1978) gave values of k ($4\pi \times \beta/\sigma$ in his terminology) measured by HeNe laser (0.6328 μm) in the laboratory. His values ranged from 0.26 for spatial ice crystals to 0.41 for aggregates.

However, further measurements by Sassen and Liou (1979) gave k as about 0.100, which is equal to the series 2 value used here.

The apparent variations in $\eta(z - z_0)$ with z, or optical depth δ, make the interpretation of the lidar backscatter in terms of the cloud optical depth that much harder. It is obvious that good data on the form of the cloud scattering phase function in natural

ice clouds is needed urgently. However, because the Monte Carlo method described in this article is very economical in time, it will be possible to make calculations on many simulated phase functions in order to determine in more detail the effects of varying both the characteristics of the forward scatter peak and the backscatter peak of the scattering phase function. Such a study is underway at present.

REFERENCES

Allen, R. J., and C. M. R. Platt, 1977: Lidar for multiple backscattering and depolarization observations. *Appl. Opt.*, **16**, 3193–3199.

Davis, P. A., 1971: Applications of an airborne ruby lidar during a BOMEX program of cirrus observations. *J. Appl. Meteor.*, **10**, 1314–1323.

Deirmendjian, P., 1964: Scattering and polarization properties of water clouds and hazes in the visible and infrared. *Appl. Opt.*, **3**, 187–196.

Dugin, V. P., B. M. Golubitskiy, S. O. Mirumyants, P. I. Paramanov and M. V. Tantashev, 1971: Optical properties of artificial ice clouds. *Izv. Atmos. Oceanic. Phys.*, **7**, 871–877.

Golubitskiy, B. M., and M. V. Tantashev, 1973: Properly conditioned use of the Monte Carlo method in solving certain optical transfer problems. *Izv. Atmos. Oceanic. Phys.*, **9**, 1213–1215.

Huffman, P., 1970: Polarization of light scattered by ice crystals. *J. Atmos. Sci.*, **27**, 1207–1208.

Jacobowitz, H., 1971: A method for computing the transfer of solar radiation through clouds of hexagonal ice crystals. *J. Quant. Spectros. Radiat. Transfer*, **11**, 691–695.

Kunkel, K. E., and J. A. Weinman, 1976: Monte Carlo analysis of multiply scattered lidar returns. *J. Atmos. Sci.*, **33**, 1772–1781.

Liou, Kuo-Nan, 1972: Light scattering by ice clouds in the visible and infrared: A theoretical study. *J. Atmos. Sci.*, **29**, 524–536.

——, R. Baldwin and T. Kaser, 1976: Preliminary experiments on the scattering of polarized laser light by ice crystals. *J. Atmos. Sci.*, **33**, 553–557.

McKee, T. B., and S. K. Cox, 1974: Scattering of visible radiation by finite clouds. *J. Atmos. Sci.*, **31**, 1885–1892.

Plass, G. N., and G. W. Kattawar, 1971: Reflection of light pulses from clouds. *Appl. Opt.*, **10**, 2304–2310.

Platt, C. M. R., 1973: Lidar and radiometric observations of cirrus clouds. *J. Atmos. Sci.*, **30**, 1191–1204.

——, N. L. Abshire and G. T. McNice, 1978: Some microphysical properties of an ice cloud from lidar observation of horizontally oriented crystals. *J. Appl. Meteor.*, **8**, 1220–1224.

——, 1979: Remote sounding of high clouds: I. Calculations of visible and infrared optical properties from lidar and radiometer measurements. *J. Appl. Meteor.*, **18**, 1130–1143.

——, and A. C. Dilley, 1979: Remote sounding of high clouds: II. Emissivity of cirrostratus. *J. Appl. Meteor.*, **18**, 1144–1150.

Sassen, K., 1978: Backscattering cross sections for hydrometeors: measurements at 6328 Å. *Appl. Opt.*, **17**, 804–806.

——, and Kuo-Nan Liou, 1979: Scattering of polarised laser light by water droplet, mixed-phase and ice crystal clouds. Part II: Angular depolarizing and multiple-scattering behavior. *J. Atmos. Sci.*, **36**, 852–861.

Wendling, P., R. Wendling and H. K. Weickmann, 1979: Scattering of solar radiation by hexagonal ice crystals. *Appl. Opt.*, **18**, 2663–2671.